



Tectonic implications of the Mw 6.8, 30 October 2020 Kuşadası Gulf earthquake in the frame of active faults of Western Turkey

Erhan ALTUNEL^{1*} , Ali PINAR² 

¹Department of Geological Engineering, Faculty of Engineering and Architecture, Eskişehir Osmangazi University, Eskişehir, Turkey

²Kandilli Observatory and Earthquake Research Institute, Boğaziçi University, İstanbul, Turkey

Received: 06.11.2020 • Accepted/Published Online: 03.01.2021 • Final Version: 16.07.2021

Abstract: A Mw 6.8 earthquake struck Western Turkey and Eastern Greece that occurred on October 30, 2020 in Kuşadası Gulf. The earthquake epicentre is located north of Samos Island and the focal mechanism solution shows that a normal fault was reactivated. The main shock and aftershock analysis imply that the large earthquake occurred on a north dipping normal fault which might be the western continuation of the Efes Fault in Western Turkey. We propose that the western continuation of the Efes Fault steps over right somewhere in northeast of Samos Island and continues further west along the northwest margin of the island, in the form of a transfer fault between two segments. The aftershock distribution shows that both the western segment and the transfer fault were reactivated during the 30 October 2020 earthquake. This fault geometry can be compared with the E-W trending Gediz Graben where the southern boundary fault steps over right around Turgutlu and continues further west in Manisa.

The historical records show that the source region and its vicinity is susceptible to frequent large earthquakes taking place on normal and strike-slip faults. The stress tensor inversion of the focal mechanisms of 55 aftershocks covering the source area shows dominant normal faulting mechanism which suggests NNE-SSW extensional stress regime in the region.

Key words: Kuşadası Gulf, 30 October 2020 earthquake, Western Turkey, Samos Island, Aegean Sea, Efes Fault

1. Introduction

The 30 October 2020 Kuşadası Gulf earthquake (Mw 6.8), that occurred in the Aegean Sea between Samos Island (Greece) in south and Seferihisar (İzmir, Turkey) in north, was felt in a wide area and resulted in loss of life and serious damage around İzmir in Western Turkey. The historical earthquake catalogues point out high seismic activity in the vicinity of the source area of the October 30, 2020 earthquake (Papazachos and Papazachou, 1997). Tan et al. (2014) reported several earthquakes of magnitude >6 around Samos since 1751 (8 earthquakes during the 19th century, and two earthquakes in the 20th century (1904 M = 6.8 and 1955 M = 6.9). Yet, another large event rocked the island recently. The source parameters of the earthquake have been determined by several seismological agencies (Table 1). The epicentre distribution of aftershocks with $M_L \geq 4.0$ is shown in Figure 1. Focal mechanism solutions of earthquakes indicate dominant normal faulting immediately north of Samos but towards west and east, strike slip component also involves faulting (Table 2, Figure 2).

The stress tensor inversion of the focal mechanisms given in Table 2 derives a stress regime acting in the source region of the 30 October 2020 earthquake. Dominant normal faulting mechanism yield a NNE-SSW extensional stress regime in the region (Figure 3). Slip distribution of the main shock shows that two segments ruptured on October 30, 2020 (Figure 4).

Since the earthquake took place in the sea offshore the northern coast of Samos Island, details of the causative fault (e.g., strike, dip, length) are not directly known. Fault parameters may be extracted using remote sensing methods but with difficulties and large uncertainties if tectonic properties of continental active faults in the adjacent area are ignored. In this paper, we provide field characteristics of active faults in the region and analyse seismic parameters of the earthquake to better understand the coseismic fault rupture associated with the October 30, 2020 earthquake.

2. Field characteristics of faults in Western Turkey

The 30 October 2020 mainshock occurred in north of Samos Island and has a seismic moment of 1.73×10^{19}

* Correspondence: ealtunel@ogu.edu.tr

Table 1. Source parameters of the October 30, 2020 mainshock as determined by different seismological agencies reported by EMSC.

Origin Time	Latitude	Longitude	Depth	Mw	Strike	Dip	Rake	Agency
30.10.2020 11:51:44	37.80	26.70	12	7.0	275	29	-87	USGS
30.10.2020 11:51:34	37.80	26.70	12	7.0	270	37	-95	GCMT
30.10.2020 11:51:27	37.90	26.80	15	7.0	97	41	-85	GFZ
30.10.2020 11:51:27	37.90	26.80	10	6.9	97	34	-85	KOERI
30.10.2020 11:51:26	37.90	26.80	10	7.2	275	45	-96	OCA
30.10.2020 11:51:26	37.80	26.80	10	7.0	289	40	-69	INGV
30.10.2020 11:51:26	37.90	26.80	14	7.0	260	36	-116	IPGP
30.10.2020 11:51:26	37.90	26.80	13	6.9	270	50	-81	UOA
30.10.2020 11:51:24	37.90	26.80	11	6.9	95	43	-87	ERD
30.10.2020 11:51:24	37.90	26.80	6	6.9	294	54	-65	NOA

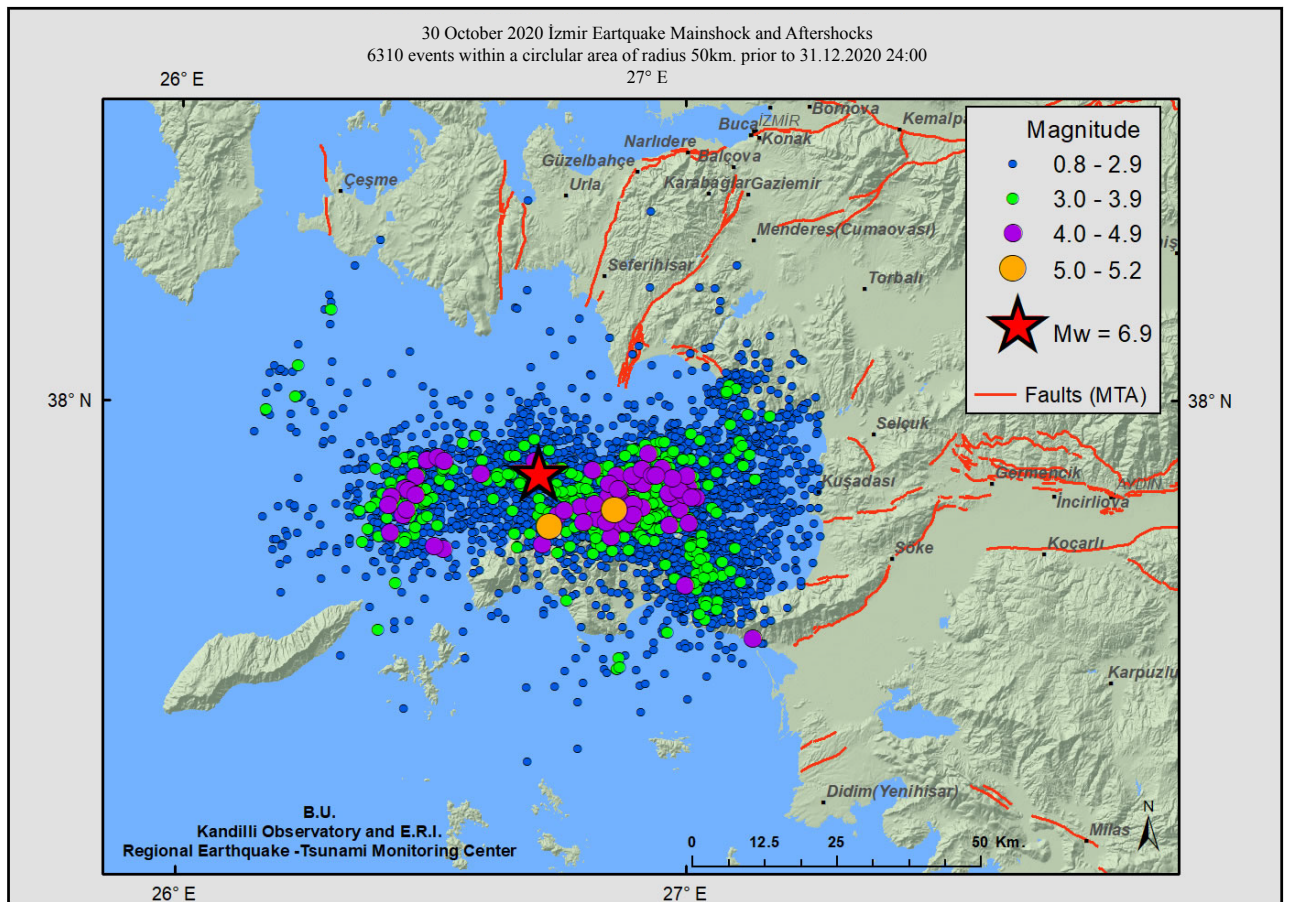


Figure 1. The mainshock location and epicentre distribution of the aftershocks around Samos Island as of November 30, 2020 (map KOERI). The mainshock is located in the mid of the aftershocks suggesting bilateral rupture propagation. The aftershock distribution is spanning an area of 50–60 km in E-W and 15–20 km in N-S directions.

Table 2. Centroid moment tensor (CMT) solutions for the aftershock during the period from October 30, 2020 to November 11, 2020. The source parameters have been retrieved using the broadband stations operated by KOERI in the frame of this study; see Pinar et al. (2003) for further details.

No	Date	Time	Latitude	Longitude	CMT Depth	Strike	Dip	Rake	Mw
1	30.10.2020	13:00	37.84	26.79	8	226	65	-177	4.9
2	30.10.2020	15:14	37.84	26.85	8	286	52	-78	5.1
3	30.10.2020	15:19	37.83	26.91	8	230	68	-151	4.7
4	30.10.2020	16:18	37.64	27.14	5	37	63	174	4.2
5	30.10.2020	16:28	37.80	26.83	4	306	67	-59	4.0
6	30.10.2020	16:37	37.92	26.48	4	85	82	-106	3.9
7	30.10.2020	16:40	37.85	26.96	12	230	74	-173	3.8
8	30.10.2020	16:47	37.89	26.92	8	236	51	-148	3.7
9	30.10.2020	17:16	37.87	27.00	9	261	38	-96	4.1
10	30.10.2020	17:47	37.89	26.95	6	267	39	-113	3.7
11	30.10.2020	18:47	37.88	26.98	6	256	40	-123	3.7
12	30.10.2020	18:59	37.88	26.39	6	353	48	-11	3.7
13	30.10.2020	19:08	37.86	26.45	6	86	86	-106	4.3
14	30.10.2020	20:35	37.79	26.52	6	42	83	178	4.3
15	30.10.2020	21:41	37.87	26.99	6	293	43	-66	4.0
16	30.10.2020	21:46	37.81	26.80	12	43	88	178	3.9
17	30.10.2020	22:37	37.81	26.89	6	276	51	-93	3.9
18	30.10.2020	22:53	37.82	26.75	4	273	31	-98	4.1
19	30.10.2020	23:05	37.79	26.86	6	287	58	-65	4.1
20	30.10.2020	23:09	37.89	26.92	12	247	55	-166	4.0
21	30.10.2020	23:33	37.85	26.86	4	242	61	-125	4.0
22	30.10.2020	23:45	37.85	26.86	4	241	57	-123	3.6
23	31.10.2020	00:20	37.81	26.96	12	323	82	-29	4.0
24	31.10.2020	01:40	37.86	26.44	4	329	69	22	4.0
25	31.10.2020	01:59	37.83	27.01	6	287	48	-72	3.7
26	31.10.2020	02:10	37.85	26.90	5	270	43	-112	4.2
27	31.10.2020	02:39	37.89	26.49	3	96	89	-110	3.7
28	31.10.2020	02:41	37.88	26.49	6	252	79	174	3.8
29	31.10.2020	04:12	37.86	26.46	3	248	78	150	3.9
30	31.10.2020	04:28	37.80	26.90	12	254	81	179	3.5
31	31.10.2020	05:22	37.82	26.80	6	296	57	-70	3.8
32	31.10.2020	05:31	37.84	26.81	6	285	48	-82	5.0
33	31.10.2020	06:34	37.84	26.93	10	265	81	-112	3.8
34	31.10.2020	12:37	37.90	26.59	8	273	83	-119	3.9
35	31.10.2020	14:42	37.88	26.47	3	96	86	-110	4.3
36	31.10.2020	16:06	37.89	26.67	2	271	87	40	4.0
37	01.11.2020	02:21	37.84	26.42	8	295	32	-88	4.0
38	1.11.2020	07:05	37.83	26.99	12	239	84	-178	4.4
39	1.11.2020	07:33	37.81	26.88	5	299	54	-71	4.6

Table 2. (Continued).

No	Date	Time	Latitude	Longitude	CMT Depth	Strike	Dip	Rake	Mw
40	2.11.2020	11:58	37.88	26.91	2	244	29	-174	4.0
41	2.11.2020	19:16	37.88	26.51	3	252	72	155	4.2
42	2.11.2020	19:39	37.72	27.05	6	257	75	-166	3.9
43	3.11.2020	18:03	37.88	26.45	5	83	80	-127	3.9
44	3.11.2020	23:17	37.70	26.99	6	20	38	146	4.1
45	3.11.2020	23:56	37.74	27.02	6	60	86	-166	3.7
46	4.11.2020	00:00	37.72	27.02	3	70	61	-168	3.9
47	4.11.2020	13:21	37.60	26.87	15	239	73	-162	3.8
48	5.11.2020	22:19	37.84	26.88	6	262	45	-101	3.9
49	6.11.2020	15:31	37.87	26.87	8	237	72	-150	3.8
50	6.11.2020	20:57	37.75	26.01	12	252	41	139	3.9
51	8.11.2020	17:56	37.87	26.60	8	277	32	-5	3.6
52	9.11.2020	04:20	37.86	26.76	6	273	43	-102	3.7
53	9.11.2020	20:30	37.89	27.00	6	296	38	-79	4.2
54	10.11.2020	02:25	39.01	27.16	6	289	57	-92	3.9
55	11.11.2020	06:49	37.88	27.00	10	245	44	-127	4.5

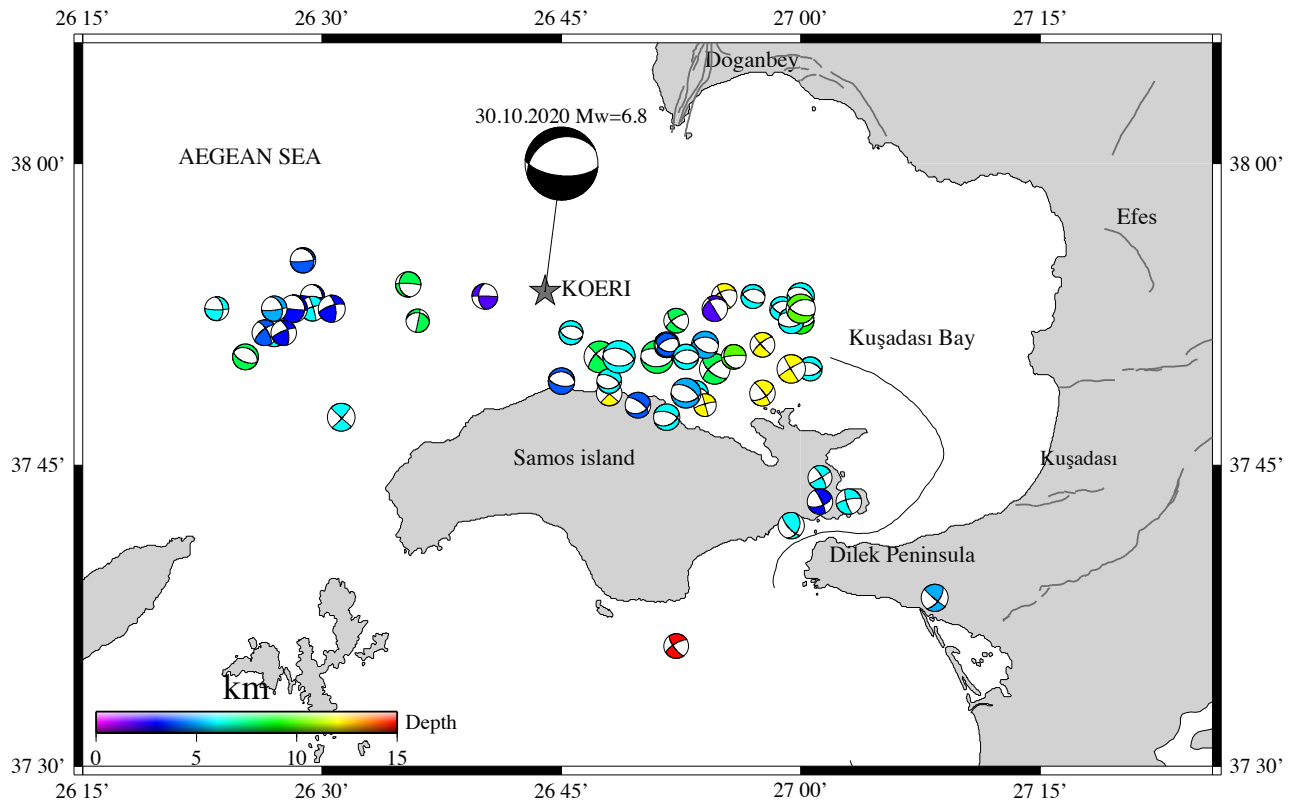


Figure 2. Focal mechanism solutions of aftershocks around Samos Island as of November 11, 2020. The faulting parameters are obtained in this study (Table 2). Star is the mainshock epicenter as determined by KOERI. The location of the aftershocks and the waveform data used to get the CMT solutions are from KOERI. The CMT inversion technique is described in Kuge (2003).

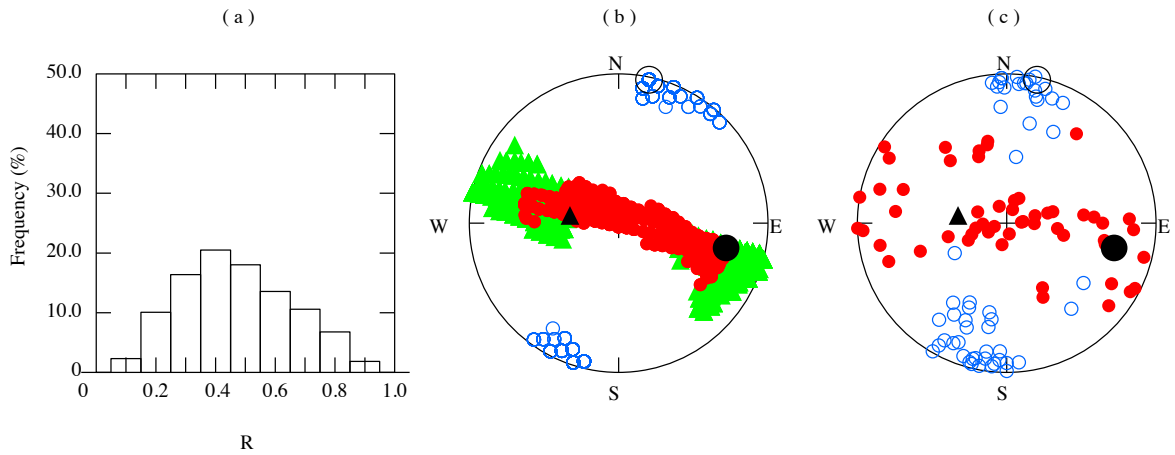


Figure 3. The results of the stress tensor analysis from the P- and T-axes of the aftershocks source mechanisms shown in Figure 2. (a) the histogram of R-values, (b) the distribution of the predicted principal stress axes and their 95 percent confidence regions and (c) the distribution of the observed P- and T-axes. In (b), red solid circles show the azimuth and plunge of the predicted maximum stress axis σ_1 , blue circles those of the predicted minimum stress axis σ_3 and green triangles those of the predicted intermediate stress axis σ_2 . In (c), red solid circles show the P-axes and blue circles the T-axes of the aftershock focal mechanisms. Black symbols denote the axes for the best stress tensor model. The best fit was obtained for $R = 0.4\text{--}0.5$ and for the azimuth and plunge pair of $(103^\circ, 27^\circ)$ for σ_1 , $(279^\circ, 63^\circ)$ for σ_2 and $(12^\circ, 2^\circ)$ for σ_3 , respectively. R is stress amplitude ratio defined as $(\sigma_2 - \sigma_1) / (\sigma_3 - \sigma_1)$; see Pinar et al., 2003 for further details.

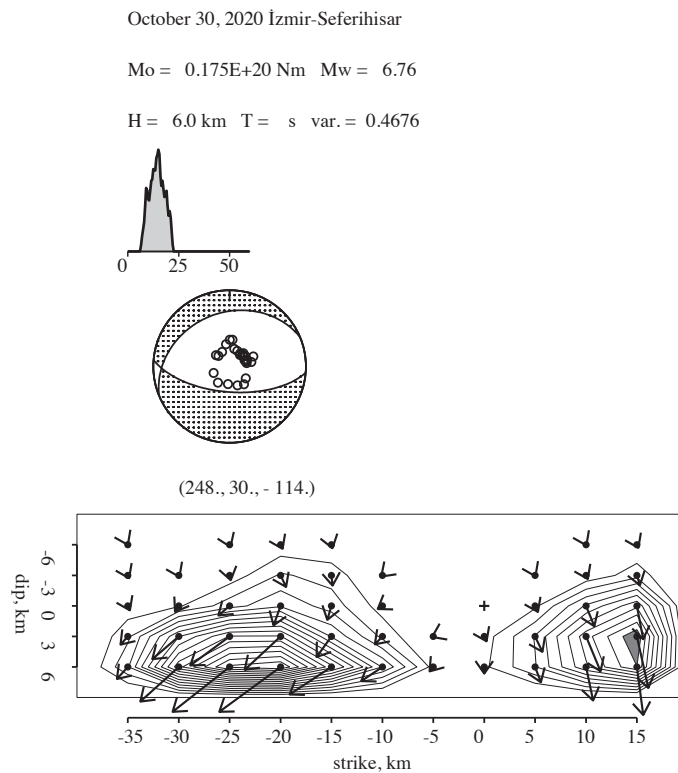


Figure 4. Moment rate of source time function (with ~ 20 s rupture length), focal mechanism (with main fault parameters: strike, dip and rake of 248, 30, -114 , respectively) and slip distribution of the October 30, 2020 Mw 6.8 earthquake (arrows are slip vectors and contour lines are interpolation of slip values determine for the grid points through teleseismic inversion of the body waves carried out in this study). The inversion results are sensitive to the selected reference depth, fault length and width. The results are shown for 50×12 km fault plane and a reference depth at 6 km. Different fault parameterizations yield different slip models.¹

¹ The University of Tokyo Earthquake Reserach Institute (2016). The name of resource (in Japanese) [online]. Website <http://www.eri.u-tokyo.ac.jp/ETAL/KIKUCHI> [6 May, 2021].

N.m. in accord with a reactivated normal fault (Figure 5). According to revised Active Fault Map of Turkey (Duman et al., 2011; Emre and Özalp 2011), major faults inland of the Turkish side are Yavansu Fault (Kuşadası Fault in Duman et al., 2011), Efes Fault, Tuzla Fault, Seferihisar Fault and Gülbağçe Fault (Figure 5). However, previous studies (e.g., Angelier et al., 1981, Hancock and Barka, 1987) proposed major faults on the east coast of the Kuşadası Gulf (Figure 6). Ocakoğlu et al. (2005) mapped some normal faults near the Turkish coast using bathymetry. Gülbağçe, Seferihisar and Tuzla faults are N-S to NE-SW trending right-lateral strike-slip faults (Emre and Özalp 2011) and both the recent 2020 earthquake sequence and related focal mechanisms are not compatible with these faults. Stiros et al. (2000) mapped normal faults in various directions both within and along the northern margin of the Samos

Island (Figure 5). Evelpidou et al. (2019) proposed a fault northern offshore of the Samos Island without giving the type of faulting (Figure 5).

The Yavansu Fault is a roughly E-W trending normal fault dipping south (Figures 6 a and 7). It is considered as the western extension of the Büyük Menderes Graben Fault but the main western strand of the graben is NE-SW trending along the Söke Fault (Figures 5 and 6). The Yavansu Fault has no geomorphic connection with the Büyük Menderes Fault. Assuming that the Yavansu Fault extends further west, it goes towards the northern margin of the Samos Island (Figure 5). Figure 5 shows major faults in Samos and it is noteworthy that there is no such fault which can be considered as the western continuation of the Yavansu Fault.

The Efes Fault is a NE-SW trending and north dipping normal fault bounding the southern part of the ancient city

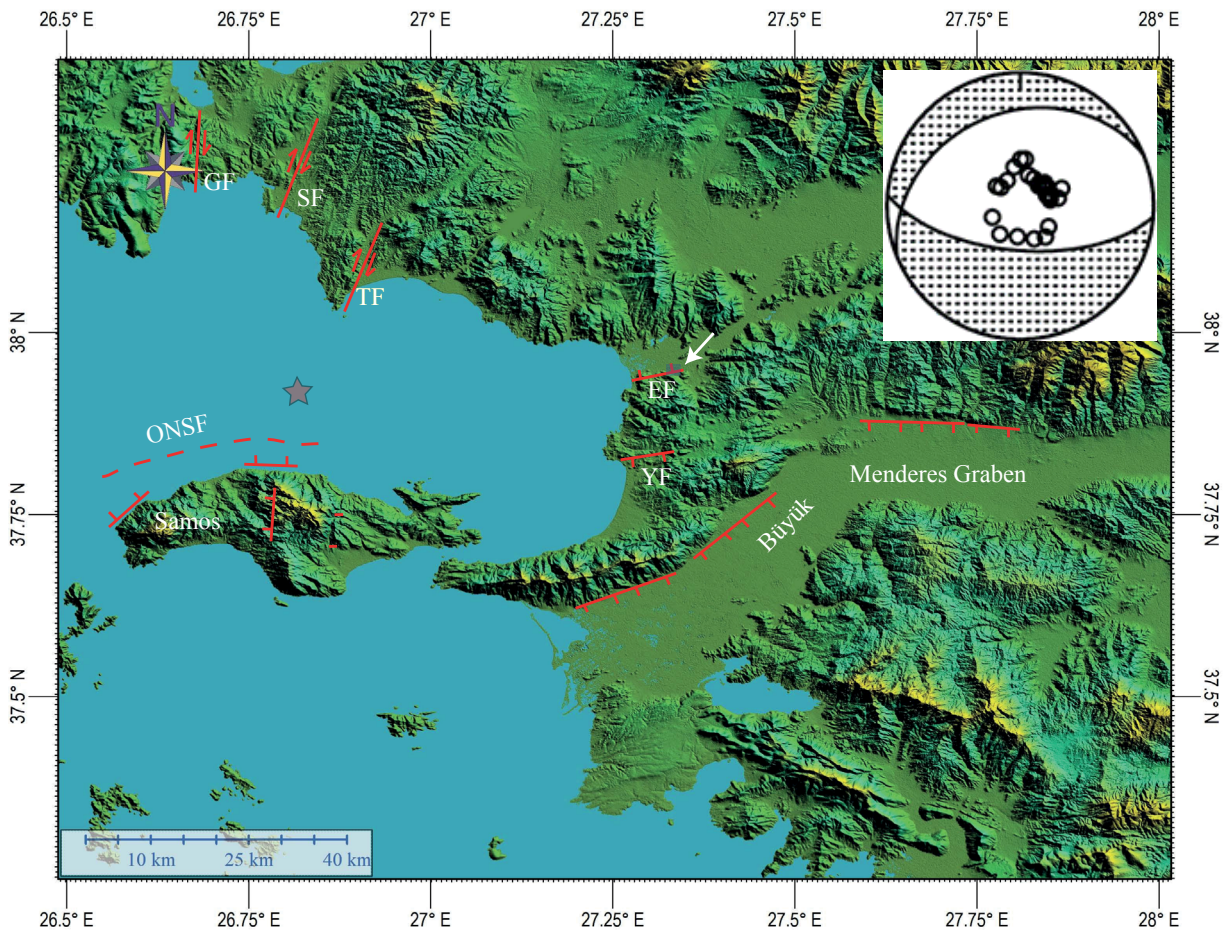


Figure 5. Major faults around the Samos Island and on the Turkish coast. Red star is the epicentre of the 30 October 2020 earthquake, inset figure is the fault plane solution by KOERI. BMF: Büyük Menderes Fault, SöF: Söke Fault, YF: Yavansu Fault, EF: Efes Fault, TF: Tuzla Fault, SF: Seferihisar Fault, GF: Gülbağçe Fault. ONSF: Offshore North Samos Fault. TF, SF and GF are from Emre and Özalp (2011), unnamed faults in Samos are from Stiros et al. (2000), ONSF is from Evelpidou et al. (2019). White arrow indicates the location of Efes (Ephesus) ancient city. DEM produced by using SRTM worldwide elevation data.

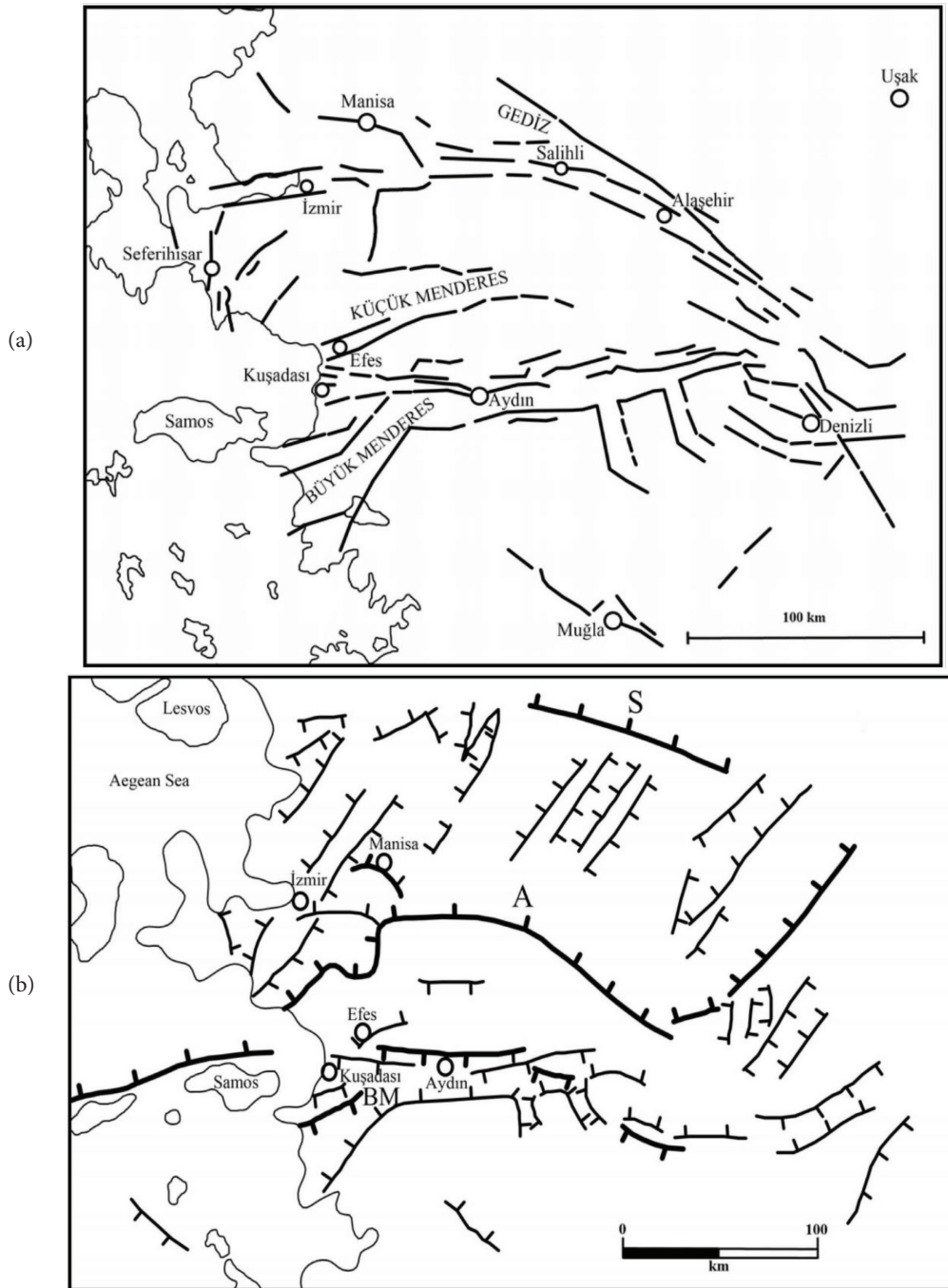


Figure 6. Maps of neotectonic faults in Western Turkey. Simplified and redrawn from; a) Angelier et al. (1981), b) Hancock and Barka (1987). Note a north dipping normal fault in north of Samos. BM: Büyük Menderes Graben, A: Gediz Graben, S: Simav Graben.

of Ephesus (Figure 8). The western part of the Efes Fault extends to WSW with WNW facing fault plane clearly visible next to the Aegean coast (Figure 8). Marine seismic sections show that the Efes Fault continues further west in the sea (Ocakoglu et al., 2005). North dipping normal faults were also mapped along the northern margin of the

Samos Island (Figures 5). Stiros et al. (2000) provided field evidence that the coast of Samos Island uplifted more than 2 m in Holocene which can be assigned to previous earthquakes. Assuming that the Efes Fault extends further west in the sea, it goes towards the Samos Island (Figure 5) but the underwater structural link is not clear.

3. Historical earthquake activity around the ancient city of Efes

According to historical catalogues (e.g., Ergin et al., 1967; Guidobani et al., 1994), major earthquakes occurred in western Turkey in historical times and some of them took place around the ancient city of Efes. For example, an earthquake destroyed the ancient cities of Efes (see Figure 5 for location) and Manisa in 44 A.D. but there is no detail information about this event. An inscription mentions destruction in Efes and adjacent cities in the 4th century A.D. and according to Altunel et al. (2001), that damage

could be related with an earthquake in the region. The 31 March 1928 earthquake (Mw 6.5) occurred in the southern margin of the Küçük Menderes Graben (Westaway, 1990) and Ambraseys (1988) reported that settlements were destroyed, and some cracks formed in the graben. However, it is difficult to attribute a specific earthquake to the Efes Fault without paleoseismological investigations. In addition, field observations in the ancient city of Efes provide evidence for possible earthquake damage in the city (Figure 9). Historical accounts, damages in the ancient city and exposed fault plane along the Efes Fault



Figure 7. A general view of the south dipping Yavansu Fault escarpment.



Figure 8. The north dipping free face (red arrows) of Efes normal fault escarpment (photograph view to the south). Relics of Efes are in the front.



Figure 9. Possible earthquake damages (blue arrows) in the ancient city of Efes. a) western wall of the Celsus Library, b) wall of one of hillside houses, c) northern entrance of the Domitian Temple (Altunel et al., 2001).

(Figure 8) are evidence for the possible reactivation of the Efes Fault in historical times.

4. Discussion

At the outset, it is noteworthy to state that existing bathymetry data shows a basin in north of Ikaria and Samos islands which is bounded by a northward facing morphological escarpment (Figure 10). The basin, which deepens westward from the Turkish coast, extends in WSW-ENE direction and reaches about 1000 m depth in northwest of Samos Island (Figure 10). Considering faults around Samos Island and on the Turkish coast, it seems that these faults belong to a fault zone which is bounding the southern margin of the basin and extending from the Efes coast in Turkey to west of Ikaria Island (Figures 5, 6a, 6b and 10). The Efes Fault in Western Turkey is the easternmost segment of this fault zone. Two segments of this fault zone offshore Samos are inferred to have reactivated during the 30 October 2020 Kuşadası Gulf earthquake.

Since the 30 October 2020 earthquake occurred in the sea, it is not possible to make direct observations to understand the kinematic of the event. The analysis of fault geometry and fault related morphology inland may contribute to understand the fault rupture geometry of the 30 October 2020 earthquake of Mw 6.8 in the Kuşadası Gulf. It is noteworthy that there is a similarity between the extension and morphology of faults around the island of Samos and the western part of the Gediz Graben (or Alaşehir Graben). As shown in Figure 11, the southern boundary fault of the Gediz Graben steps over to the right in west of Turgutlu town and continues in the same westward direction in Manisa. The slip on the fault in Turgutlu is transferred to the Manisa Fault by the NW-SE trending fault. As indicated in Figures 5 and 6b, there are north dipping normal faults along the northern margin of Samos Island. Assuming that the Efes Fault continues further west in the sea to connect with faults in north of Samos Island, there should be a step over to the right somewhere in northeast of the island (Figure 11). The slip

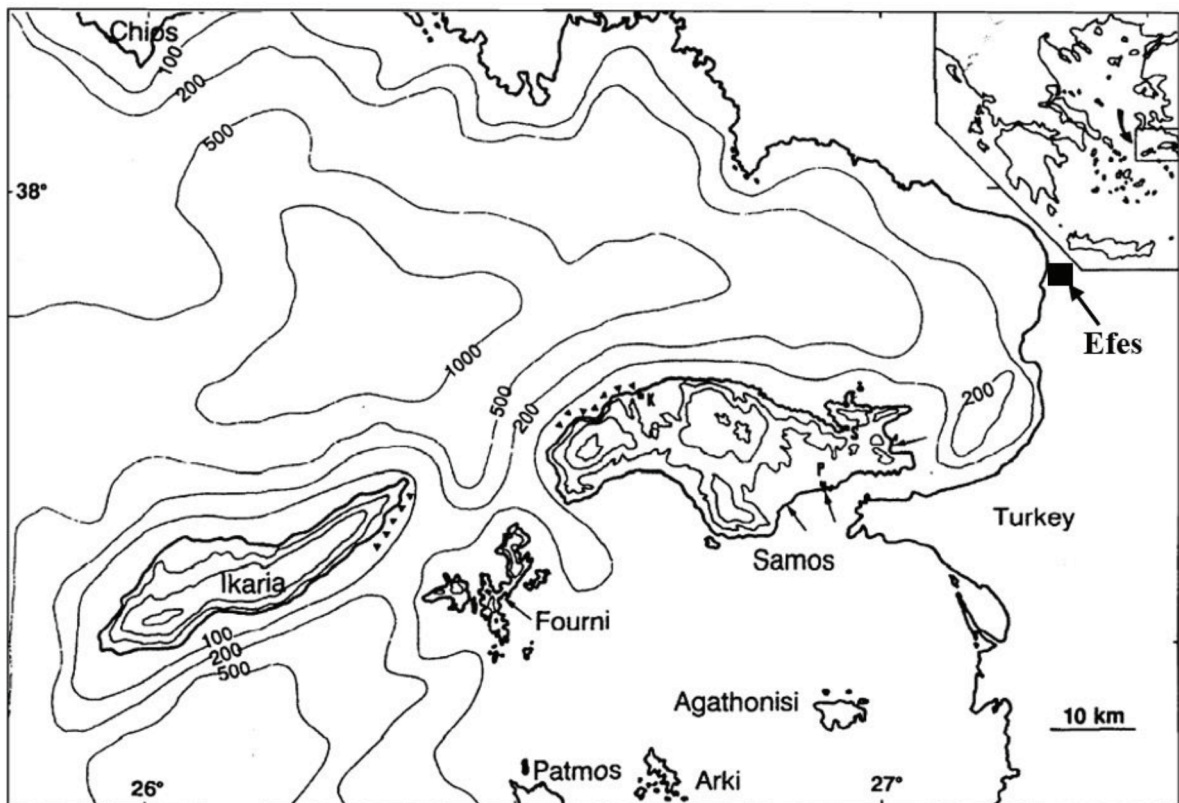


Figure 10. Topography and bathymetry in the Samos-Ikaria area. Contours of 200, 500 and 1000 m are shown (Stiros et al., 2000).

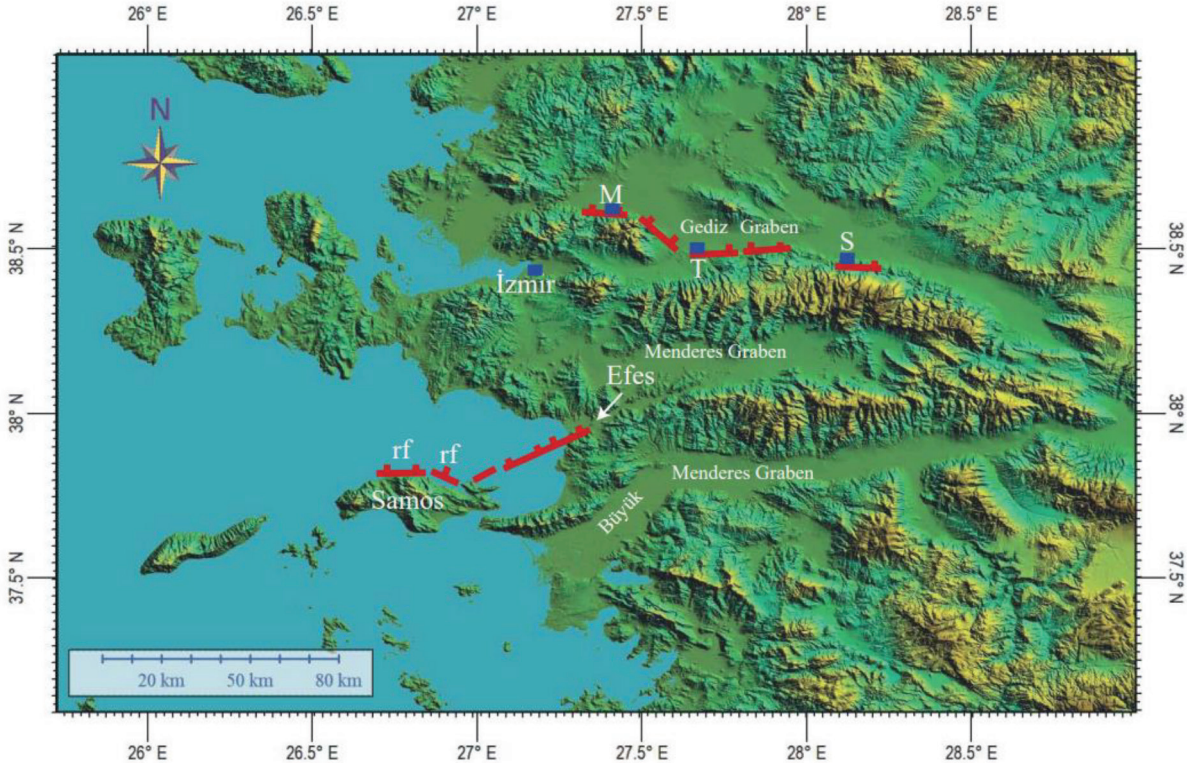


Figure 11. Major faults in the western part of the Gediz Graben (around Manisa) and proposed fault model geometry around Samos Island that illustrates fault rupture of 30 October 2020 earthquake (M_w 6.8) (faults indicated by rf were ruptured during 30 October 2020 events). M: Manisa, T: Turgutlu, S: Salihli (DEM produced by using SRTM worldwide elevation data).

on the western part of the Efes Fault is transferred to the fault in north of Samos Island by a NW-SE trending normal fault such as in the western part of the Gediz Graben. Based on epicentre distribution of seismic activity (Figures 1 and 2), it is possible that the fault in north of Samos and the transfer fault were reactivated during the 30 October 2020 event. The InSAR model developed by Akoğlu and Çakır (2020)¹ also suggests the reactivation of a NW-SE-trending and north dipping fault in north of Samos which may corresponds with the suggested transfer fault (Figure 12). In conclusion, we propose that if the reactivated fault in north of Samos continues towards east, it corresponds with the north dipping Efes Fault in the Turkish coast.

¹ Akoğlu AM, Çakır Z (2020). InSARcat 30/10/20 Aegean Sea (Sisam/Samos Island-Gulf of Kuşadası) earthquake rapid InSAR processing results [online]. Website https://web.itu.edu.tr/akoglua/depem/2020/30102020_Sisam.php [accessed 15 December 2020].

Considering that the eastern extent of the reactivated fault is the Efes Fault, it is possible that the densely populated touristic region of Western Turkey is the location of the similar size future earthquake.

Acknowledgment

Our special thanks go to Prof. Mustafa Erdik and Prof. Sinan Akkar, who encouraged us to write this article and read the first version. We are grateful for helpful comments and constructive reviews by Mustapha Meghraoui, Özgür Kozacı and two anonymous reviewers which improved our manuscript. We thank Prof. C. Çağlar Yalçiner for producing DEMs and Mohammed Hayyas and Yunus Can Kurban for redrawing some figures.

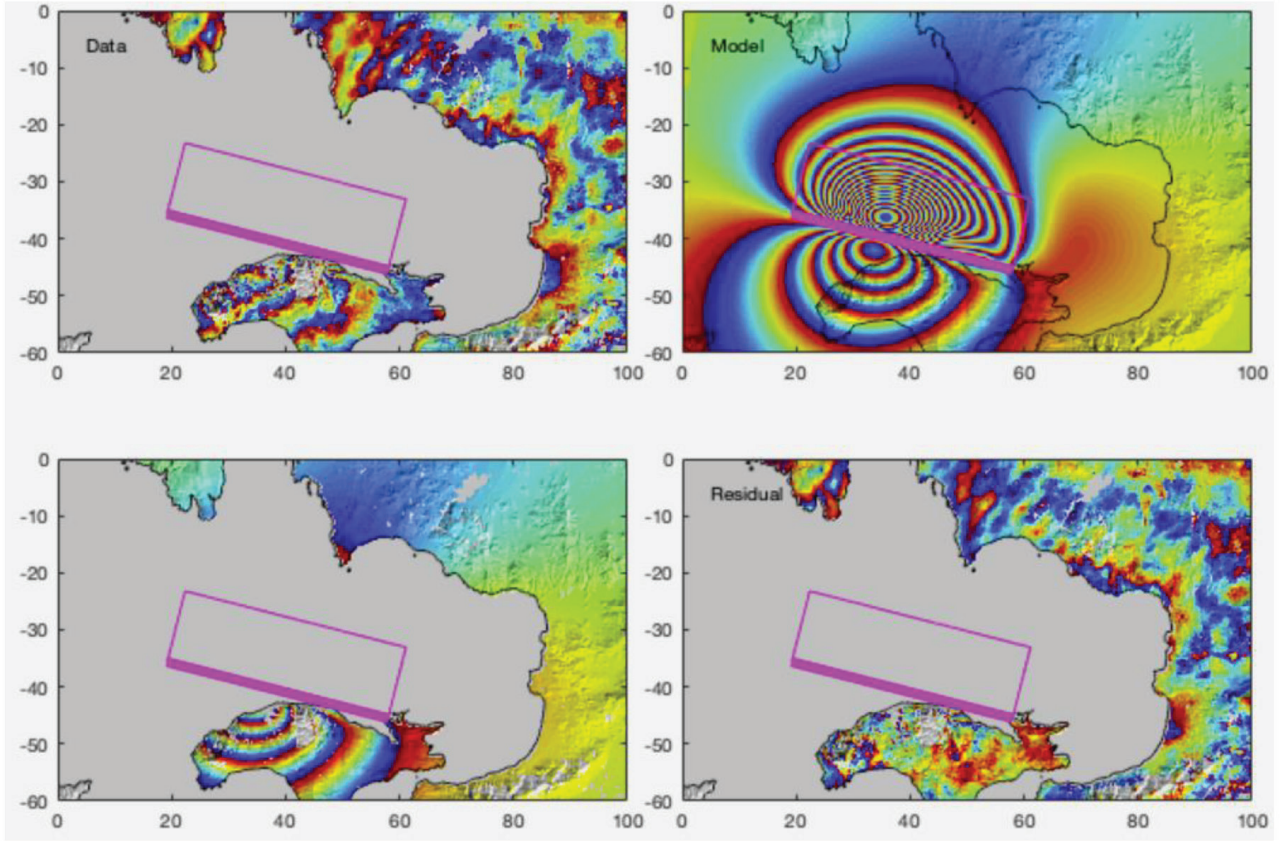


Figure 12. Fault model from InSAR data suggesting a WNW-ESE trending and north dipping fault.¹

References

- Altunel E, Barka A, Akyüz S (2001). Gediz ve Küçük Menderes Grabenindeki Antik Kentlerde Tarihsel Deprem Hasarlarının Araştırılması ve İncelenmesi. (*Investigation and examination of historical earthquake damages in ancient cities located along the Gediz and Küçük Menderes grabens*). TÜBİTAK Projesi, Proje No: YDABÇAG199-Y098. Ankara, Turkey: TÜBİTAK.
- Ambraseys NN (1988). Engineering seismology: part II. Earthquake Engineering and Structural Geodynamics 17: 1-105.
- Angelier J, Dumont JF, Karamandereci H, Poisson A, Şimşek Ş et al. (1981). Analyses of fault mechanisms and expansion of southwestern Anatolia since the late Miocene. Tectonophysics 75: T1-T9.
- Duman TY, Emre Ö, Özalp S, Elmacı H (2011). 1:250 000 Scale Active Fault Map Series of Turkey, Aydın (NJ 35-11) Quadrangle. General Directorate of Mineral Research and Exploration, Serial Number: 7. Ankara, Turkey: General Directorate of Mineral Research and Exploration.
- Emre Ö, Özalp S (2011). 1:250 000 Scale active Fault Map Series of Turkey, Urla (NJ 35-6) Quadrangle. General Directorate of Mineral Research and Exploration, Serial Number: 5. Ankara, Turkey: General Directorate of Mineral Research and Exploration.
- Ergin K, Güçlü U, Uz Z (1967). A Catalogue of Earthquakes for Turkey and Surrounding Area (11 A.D.–1964 A.D.). İstanbul, Turkey: ITU, Institute of Geophysics.
- Evelpidou N, Pavlopoulos K, Vouvalidis K, Syrides G, Triantaphyllou et al. (2019). Holocene palaeogeographical reconstruction and relative sea-level changes in the southeastern part of the island of Samos. Geoscience 351: 451-460.
- Guidoboni E, Canastari A, Traina G (1994). Catalogue of Ancient Earthquakes in the Mediterranean Area Up to the 10th Century A.D. Rome, Italy: Istituto Nazionale Geophysics and Volcanology.

- Hancock PL, Barka AA (1987). Kinematic indicators on active normal faults in western Turkey. *Journal of Structural Geology* 9 (5/6): 573-584.
- Kuge K (2003). Source modeling using strong-motion waveforms: toward automated determination of earthquake fault planes and moment-release distributions. *Bulletin of the Seismological Society of America* 93: 639-654.
- Ocañoğlu N, Demirbağ E, Kuşçu İ (2005). Neotectonic structures in İzmir Gulf and surrounding regions (Western Turkey): evidences of strike-slip faulting with compression in the Aegean extensional regime. *Marine Geology* 219: 155-171.
- Papazachos B, Papazachou C (1997). *The Earthquakes of Greece*. Thessaloniki, Greece: Ziti Publications.
- Pınar A, Honkura Y, Kuge K (2003). Moment tensor inversion of recent small to moderate sized earthquakes: implication for seismic hazard and active tectonics beneath the Sea of Marmara. *Geophysical Journal International* 152: 1-13.
- Stiros S, Labrel-Deguen F, Papageorgiou S, Evin J, Pirazzoli PA (2000). Seismic coastal uplift in a region of subsidence: Holocene raised shorelines of Samos Island, Aegean Sea, Greece. *Marine Geology* 170: 41-58.
- Tan O, Papadimitriou EE, Pabuccu Z, Karakostas V, Yörük A et al. (2014). A detailed analysis of microseismicity in Samos and Kusadasi (Eastern Aegean Sea) areas. *Acta Geophysica* 62 (6): 1283-1309.
- Westaway R (1990). Blockrotation in western Turkey: 1. observational evidence. *Journal of Geophysical Research* 95: 19857-19884.